Available online at www.sciencedirect.com

ScienceDirect

Underground Space 9 (2023) 20–30

www.keaipublishing.com/undsp

Effect of stress path on the mechanical properties of calcareous sand

Houzhen Wei [a], Hao Liu [a,b,c], Xiaoxiao Li [a], Zhao Tao [d], Yongjie Wu [a], Jianhua Shen [a], Mei Yin [d,*]

[a] State Key Laboratory of Geomechanics and Geotechnical Engineering, Institute of Rock and Soil Mechanics, Chinese Academy of Sciences, Wuhan 430071, China

[b] College of Civil Engineering and Architecture, Guilin University of Technology, Guilin 541004, China

[c] Guangxi Key Laboratory of Geomechanics and Geotechnical Engineering, Guilin University of Technology, Guilin 541004, China

[d] Dept. of Civil and Environmental Engineering, Brunel University London, London UB8 3PH, UK

Received 20 January 2022; received in revised form 29 May 2022; accepted 26 June 2022
Available online 1 October 2022

Abstract

Calcareous sand is widely observed in the foundation of off-shore infrastructure. Although a lot of research has been carried out on the mechanical properties of calcareous sand, study into the influence of the stress–strain path on the mechanical behaviour of calcareous sand is very limited. In this study, a series of triaxial tests were performed on calcareous sand under three different stress paths. The particle morphology of calcareous sand before and after the tests, the stress–strain relationship under different stress paths, and the characteristics of shear strength and deformation were investigated. The results show that the consolidation pressure and stress path have significant effects on the volume strain, strength, and particle breakage of calcareous sand. In addition, the underlying mechanisms of the different behaviours of calcareous sand observed in this study were discussed.

Keywords: Calcareous sand; Triaxial test; Stress path; Particle breakage

1 Introduction

Over the last few decades, concern has been raised about the foundation design, construction, maintenance, and decommissioning of offshore infrastructure. (Bai & Bai, 2018). Calcareous sand is widely observed in the foundation of this infrastructure. Because of the differences in minerals, micro-structures, and particle shapes, calcareous sand is believed to be associated with distinctive mechanical properties compared with quartz sand (Jafarian et al., 2018). Therefore, many scholars have carried out research to investigate the unique mechanical properties of calcareous sand (Airey et al., 2011; David Frost et al., 2012; Shahnazari & Rezvani, 2013; Fukuoka et al., 2007; Altuhafi & Coop, 2011; Miao & Airey, 2013; Wu et al., 2014; Yu, 2017; Wei et al., 2021).

Calcareous sand has high porosity due to the effect of particle interlocking and high intra-granular void ratios (Coop & Atkinson, 1993). Based on 1D compression tests, Altuhafi and Coop (2011) investigated the effect of breakages on calcareous sand. It was found that the soil behaviour due to the particle breakage during yielding was associated with the particle shape and surface roughness. Similar results were obtained by Einav (2007). Unlike quartz, which is quite hard and resistant to abrasion (Powrie, 2004), calcareous sand can be fragmented easily even under a low stress (Wei et al., 2018). By conducting triaxial tests, the mechanical behaviour of calcareous sand was revealed by Coop (1990) and Fahey and Jewell (1988). They found that the sand tended to have a constant volume and a constant deviator stress under the drained condition, and the yield surface was closely related to the confining stress. Using similar tests, Zhang et al. (2009, 2008) presented that the particle breakage and dilatancy have significant effects on the shear strength of calcareous sand.

* Corresponding author.
E-mail address: mei.yin@brunel.ac.uk (M. Yin).

https://doi.org/10.1016/j.undsp.2022.06.003

He et al. (2018) investigated the effect of particle breakage on the shear strength of calcareous sand using a series of ring shear tests. It was found that particle breakages could effectively reduce the shear strength of the calcareous sand. Chai et al. (2019) and Yang et al. (2019) proposed a term of critical shear rate. They explained that the shear strength and the friction angle of calcareous sand decreased with the shear rate below the critical shear rate. In addition, Yan et al. (2020) investigated the effects of confining pressure and particle size on the shear strength of calcareous sand using triaxial shear tests.

Although a lot of research has been carried out on the mechanical properties of calcareous sand, most studies focus on the confining stresses, shear rates, void ratios, gradation, and particle sizes, etc. The influence of the stress–strain path on the mechanical behaviour of calcareous sand, however, has not been extensively investigated. The investigation of the behaviours of calcareous sand under different stress paths is of great significance, which can provide a scientific basis for offshore construction and offer guidance for engineering practice. Therefore, this paper presents triaxial tests carried out to investigate the stress–strain relationship, shear strength, and particle breakage of calcareous sand under different stress paths. In addition, the underlying mechanisms of the different behaviours of calcareous sand observed in this study are discussed.

2 Triaxial test

In this study, a series of tests were conducted using the Triaxial Automated System TAS-LF (shown in Fig. 1) to investigate the mechanical behaviours of calcareous sand under different stress paths. Because of the high permeability of the sample, only the drained condition was considered. Three types of stress paths were applied to the samples, including the conventional triaxial tests (CTC), constant mean stress tests (TC), and the constant stress ratio tests (PL), as shown in Table 1. The stress increments were controlled at $\Delta\sigma_1/\Delta\sigma_2 = 2.7$ and 3.0, corresponding to the stress increment ratios $\Delta q/\Delta p = 1.08$ and 1.20 (p is the average principal stress, and q is the deviator stress), as shown in Fig. 2.

The calcareous sand was obtained from South China Sea. Prior to the triaxial tests, the sand was washed using distilled water and dried in an oven, then sieved to select the particles with diameters from 1–2 mm as the specimen used in the work. To quantify the shear behaviour of the calcareous sand, measurements were taken to obtain the physical properties of the specimen, e.g., the specific gravity $G_s = 2.82$, the maximum dry density $\rho_{dmax} = 1.31$ g/cm^3, and the minimum dry density $\rho_{dmin} = 0.79$ g/cm^3. During the tests, two sets of samples with different initial relative densities (D_r) of 0.6 and 0.8 were isotopically consolidated under the stress σ_c of 100, 200, 400, and 800 kPa, respectively. Then for each consolidated sample, the three types of stress paths (CTC, TC and PL) were applied individually until the samples were sheared to fail, which was used to determine the shear strength of each sample. The summary of the triaxial tests is listed in Table 2.

The sieve analysis test was carried out to select sand particles with size of 1–2 mm. The selected sand was trimmed into a cylindrical specimen with a diameter of 61.8 mm and

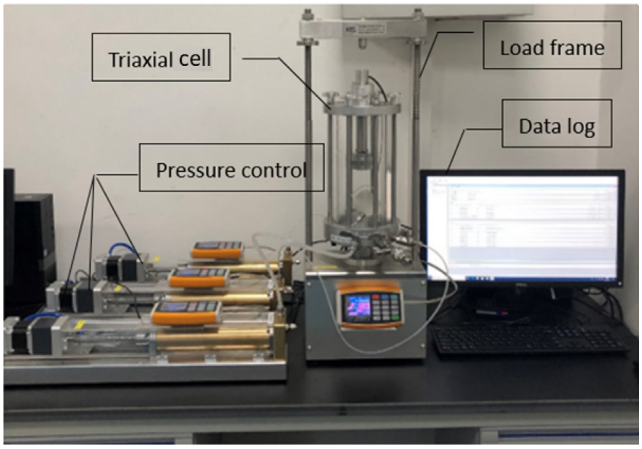

Fig. 1. TAS-LF Triaxial Automated System.

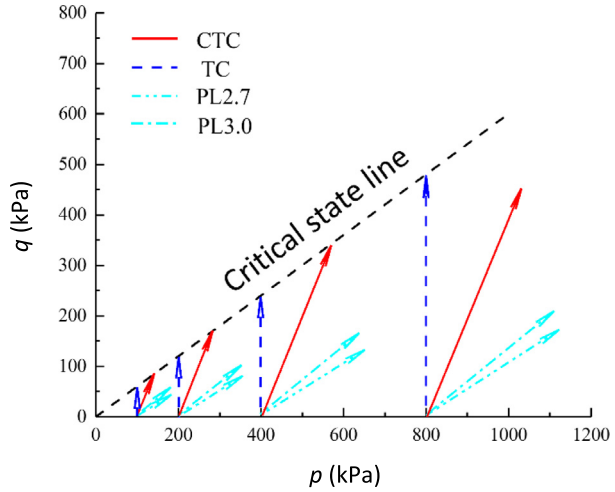

Fig. 2. Stress paths in p-q space.

Table 1
Three types of stress paths.

Stress path	Consolidation pressure	Vertical stress
Conventional triaxial tests (CTC)	$\sigma_1 = \sigma_2 = \sigma_3$	$(\Delta\sigma_1 + \sigma_1) > \sigma_3$ $\sigma_1' > \sigma_1$
Constant mean stress tests (TC)	$\sigma_1 = \sigma_2 = \sigma_3$	$\sigma_1 > \sigma_2 = \sigma_3$, $\Delta\sigma_1 = \sigma_3/2$
Constant stress ratio tests (PL)	$\sigma_1 = \sigma_2 = \sigma_3$	$\Delta\sigma_1/\Delta\sigma_3 = k$, $k > 1$, $\Delta\sigma_3 > k > 1$, $\Delta\sigma_3 > 0$

Table 2
Summary of the triaxial tests.

Test ID	Stress increment ratio		Consolidation pressure σ_c/kPa	Stress path	Loading method	Shear rate	Termination
	$\Delta\sigma_1/\Delta\sigma_3$	$\Delta q_1/\Delta p$					
CTC100	∞	3	100	σ_1 increases	CTC	$\Delta\varepsilon_a = 0.06$ mm/min	$\varepsilon_a = 20\%$
CTC200			200	$\sigma_3 = \sigma_c$ = constant			
CTC400			400				
CTC800			800				
TC100	−2	∞	100	σ_1 increases	TC	$\Delta\sigma_1 = 2$ kPa/min	
TC200			200	σ_3 decreases			
TC400			400	$p = \sigma_c$ = constant			
TC800			800				
PL2.7	2.7	1.08	100	σ_1 increases	PL	$\Delta\sigma_3 = 1$ kPa/min	
			200	σ_3 increases			
			400				
			800				
PL3.0	3.0	1.20	100				
			200				
			400				
			800				

a height of 120 mm, then sealed within a rubber membrane placed in a triaxial cell. After that, the sand sample was saturated, consolidated, and sheared under different stress paths. In order to investigate the mechanical behaviours of calcareous sand, two groups of sand samples with relative densities of 0.6 and 0.8 were set up.

In order to investigate the influence of particle breakage on the mechanical behaviours of the sand, the relative breakage potential was calculated before and after the triaxial tests based on the effect of particle size distribution (Hardin, 1985).

$$B_r = \frac{B_t}{B_{P0}}, \tag{1}$$

where B_r is the relative breakage potential, B_t is the total breakage potential, and B_{P0} is the initial breakage potential. The calculation method is illustrated in Fig. 3, where S_1 is the area ACD and S_2 is the area ABC.

$$B_t = S_2 \tag{2}$$

$$B_{p0} = S_1 + S_2 \tag{3}$$

$$B_r = B_t/B_{P0} = S_2/(S_1 + S_2) \tag{4}$$

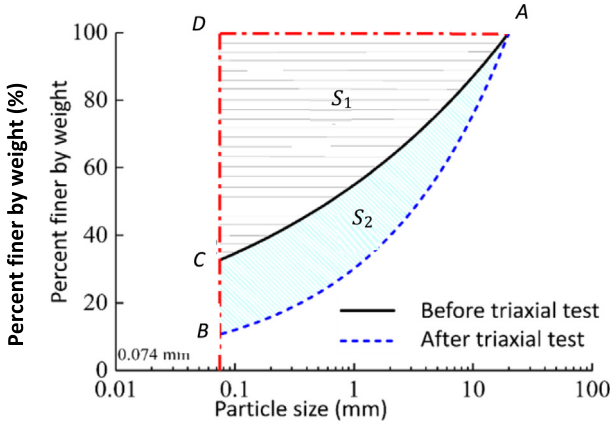

Fig. 3. Calculation of breakage potential.

3 Results and discussion

3.1 Stress–strain relationship

Figure 4 shows the relationships between the deviator stress and the axial strain of the two groups of sand samples ($D_r = 0.6$ and $D_r = 0.8$) under three different stress paths. As shown in the CTC (Fig. 4(a)) and TC tests (Fig. 4(b)), the deviator stress increases with the axial strain until it reaches the peak point. Then as the strain continually develops, the deviator stress decreases, indicating the strain-softening behaviour of the samples. It is also noted that the deviator stress reaches its peak strength at a smaller strain for the smaller confining pressure, and a larger confining pressure results in a larger peak strength. The strain softening behaviour is more noticeable under a lower confining pressure. Although a similar tendency is observed in the TC tests, the change of deviator curves tends to become small after the strain of 8%.

The samples in the PL tests, however, show completely different behaviour as seen in Fig. 4(c) and (d). Figure 4 (c) and (d) depicts the stress–strain relationship of the two groups of sand samples under the stress paths with the $\Delta\sigma_1/\Delta\sigma_3$ ratio of 2.7 and 3 ($q/p = 1.08$ and 1.12) respectively. It is found clearly that the deviator stress increases with the axial strain without any peak or turning points, implying the strain hardening behaviour of the tested samples in PL tests. The dense sand tends to have a larger strain under the same stress. All the tests were terminated when the strain approached 20%, where no distinct residual strength was observed.

Figure 5 shows the relationship between volumetric strain (ε_v) and axial strain (ε_a) for different stress paths. In the CTC and TC tests, all the sand samples showed initial contractive behaviour, followed by a dilatancy phase. It should be noted that an exception in the CTC tests is the confining pressure of 800 kPa. In the CTC tests, as the confining pressure increases to 400 kPa and above, more sand

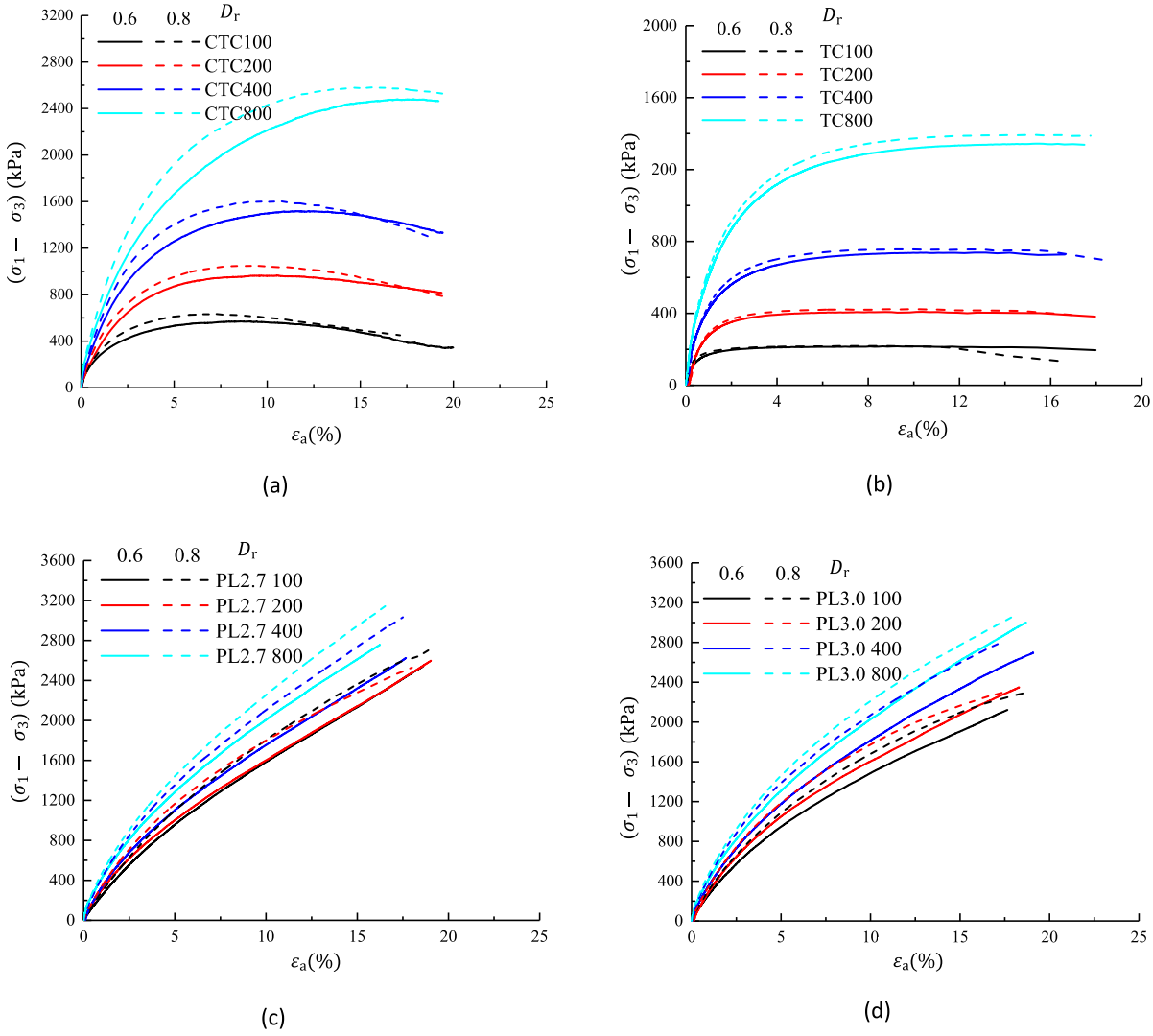

Fig. 4. Relationships between the deviator stress and the axial strain under different stress paths: (a) CTC, (b) TC, (c) PL2.7, and (d) PL3.0.

particles tend to break, resulting in a decrease of volume. Therefore, the dilatancy becomes less significant compared with the samples with lower confining stresses applied (100 kPa and 200 kPa). In the TC and CTC tests, the dense sand particles remained intact and interlocked, so they did not have the freedom to move around one another. During the loading process, a lever motion occurred between neighbouring particles, which resulted in bulk expansion of the sand. This also indicates that the denser sand sample had a tendency to dilate as it was sheared under the identical stress path, as shown in Fig. 5(b). Therefore, dilatancy is a dominant behaviour of samples under TC stress conditions.

By contrast, Fig. 5(c) and (d) shows the contraction r of sand samples only in PL tests. This also indicates shear behaviours of the calcareous sand independent of the initial void ratio. From the results, it can be seen that the sand samples become more compressible under the stress path $\Delta\sigma'_1/\Delta\sigma'_3$ ratio of 2.7. This is because both the axial stress σ'_1 and the confining pressure σ'_3 were scaled up in the PL tests. The axial stress increment restrained the movement of the sand particles. The sand sample was simultaneously compacted due to the incremental stress in the vertical direction, resulting in stronger interlocking between particles so a smaller deformation of soil samples was observed. However, as the stresses σ'_1 and σ'_3 increased, the sand particles began to break. Those smaller particles tended to fill up the void to achieve a more compacted sample.

As shown in Fig. 5, the inflection point on each curve represents the point where the contraction stage transits to the dilation stage, and it is named the dilative point. As illustrated in Fig. 4, the peak point on each curve is called the softening point which represents the peak strength of the calcareous sand. To investigate the effect of the initial void ratio on the stress–strain relationship, the axial strains corresponding to the dilative points and softening points are plotted in Fig. 6. Under the same load, the axial strain at the dilative point is smaller than that at the softening point, which is consistent with the deformation of the contractive stage followed by the dilatancy

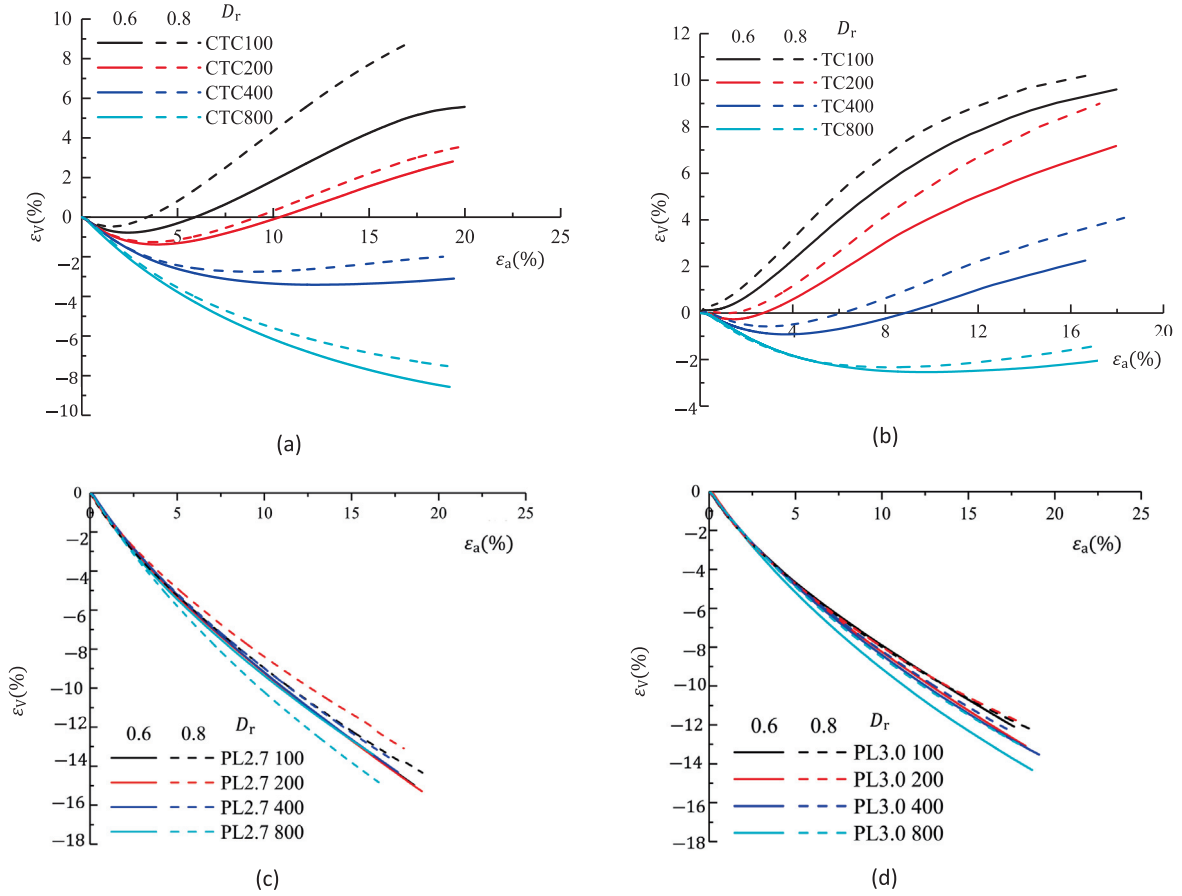

Fig. 5. Relationship between volumetric strain (ε_v) and axial strain (ε_a) for different stress paths: (a) CTC, (b) TC, (c) PL2.7, and (d) PL3.0.

observed in the triaxial tests. It can also be found that the axial strains at the dilative and softening points of the loose sand ($D_r = 0.6$) are larger that of the dense sand ($D_r = 0.8$).

Figure 7(a) and (b) depicts the relationship between the volumetric strain (ε_v) and confining pressure at the dilative point and the softening point. It is shown that the contraction is amplified by increasing the confining pressure. For different void ratios, the denser sample leads to a smaller volumetric strain at the dilative point. The same trend was observed in terms of the softening point strain versus the confining pressure, as shown in Fig. 7(b). However, it should be noted that both dilatancy and contraction appeared at the softening point. It can be explained that under a lower confining pressure the sample tends to dilate more compared with that under a higher confining pressure. In addition, higher relative density leads to larger dilations during the tests.

It should be noted that the effect of stress path on the calcareous sand behaviour is more significant for medium dense sand and dense sand. The loose sand contains larger pore spaces. These pore structures are easily broken, filled by small sand particles. This process is shown in the contraction stage observed in the tests. After that, the smaller-sized particles congregate and fill up the pore spaces, stabilizing and enlarging the soil microstructure, producing the dilatancy seen in the CTC and TC tests. On the other hand, the behaviour of dilatancy is quite different under different stress paths. This is because the dilatancy is related to the deviator stress $\sigma_1 - \sigma_3$. In the TC tests, dilatancy is more significant than in the CTC test. This is because that in the TC tests the deviator stress applied to the sample is the largest compared with the CTC and PL tests, and this causes more particle breakage. While in the PL test, both the axial stress and the confining pressure increase by the ratio $\Delta\sigma_1/\Delta\sigma_3 = 2.7$ and 3.

3.2 Effect on shear strength

The effect of stress paths on the shear strength of calcareous sand was investigated. Figure 8 shows the deviator stresses versus confining pressure at the dilative point and softening point. It is shown that the deviator stress is affected by stress paths. It increases with the confining pressure at the dilatancy point and the softening point.

Figure 9 shows the deviator stress versus consolidation pressure at the peak point. Again, the deviator stress increases with the consolidation pressure and the initial density. However, the consolidation pressure has the largest impact on the CTC test and the least impact on the PL test. The deviator stresses are largest in the PL test

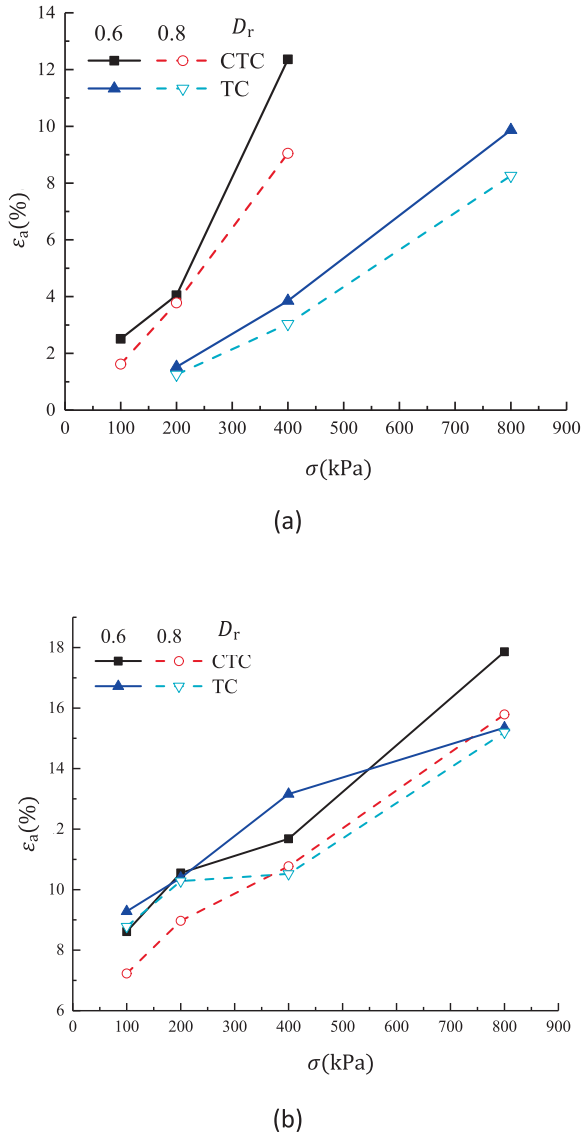

Fig. 6. Axial stress versus confining pressure at the dilative point and softening point for different relative densities: (a) Axial stress at the dilative point, and (b) axial stress at the softening point.

and smallest in the TC test under the same confining pressure and initial density. This indicates that the stress path has a large impact on the peak strength of calcareous sand. During the shearing process, the shear strength is dependent on the particle–particle contacts. A dense sample with more particles is expected to have higher shear strength.

By plotting the Mohr circle of effective stress at both peak point and the final state, soil strengths can be expressed as angles of shearing resistance. According to the Mohr–Coulomb failure criterion, the effective friction angle can be obtained by

$$\sin\varphi = \frac{\sigma_1/\sigma_3 - 1}{\sigma_1/\sigma_3 + 1} \tag{5}$$

The peak friction angle φ_p and the lower steady state friction angle or the final friction angle (at the end of the

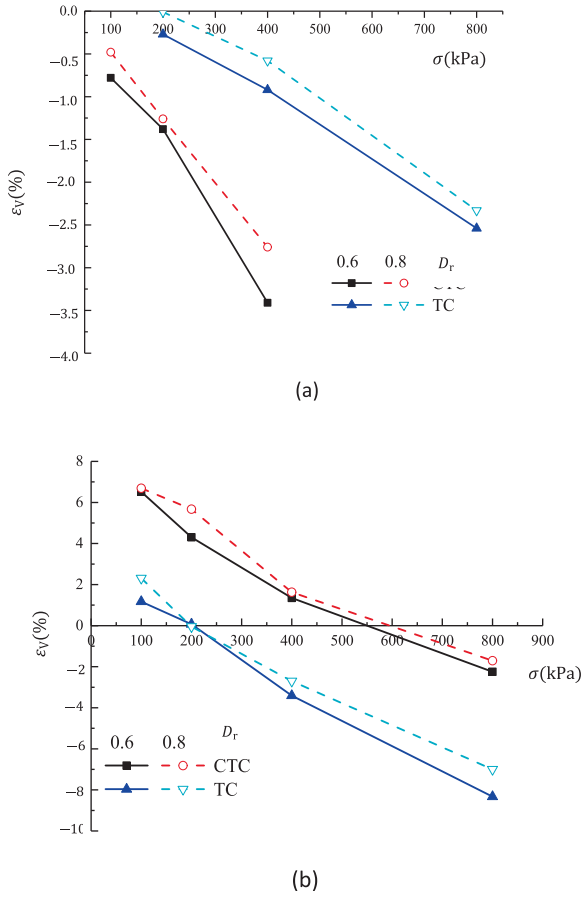

Fig. 7. Volumetric strain versus confining pressure at the dilative point and softening point for different relative densities: (a) Volumetric strain at the dilative point, and (b) volumetric strain at the softening point.

test at $\varepsilon_a = 20\%$) φ_f are given by the peak principal stress ratio R_{max} and the final principal stress ratio R_f.

$$R_{max} = \frac{\sigma_{1max}}{\sigma_{3max}} \tag{6}$$

$$R_f = \frac{\sigma_{1f}}{\sigma_{3f}} \tag{7}$$

The calculated values of the peak friction angle φ_p and the final friction angle φ_f from the CTC and TC tests are plotted in Fig. 10. Under the same stress condition, the values of φ_p increase with the initial density, but decrease as the confining pressure decreases. However, the effect of confining pressure on φ_p is more significant than the effect of the initial density. For the samples with the same initial density and pre-consolidation pressure, the values of φ_p change with different stress paths. The variation of φ_p between the CTC and TC tests is about 1°–6°. A similar trend is also found in the final friction angle φ_f. The change of friction angle of quartz sand under different stress paths is very limited, so the calcareous sand behaves different from the quartz sand.

Duncan and Chang (1970) proposed a nonlinear model to describe the stress–stain behaviour of soil. In this model, φ_p can be derived from the consolidation pressure:

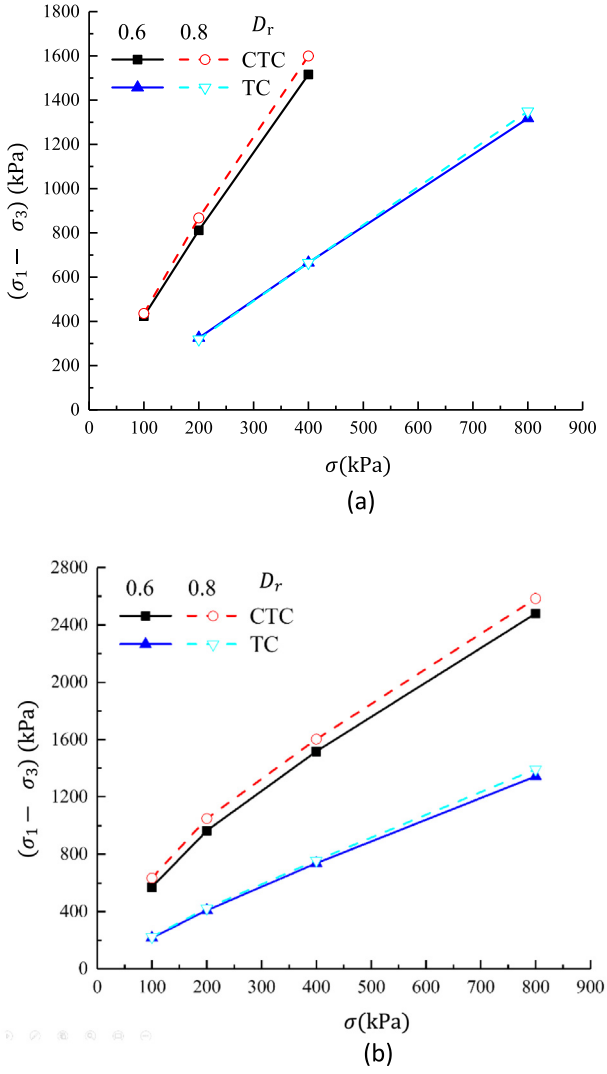

Fig. 8. Deviator stresses versus confining pressure at: (a) Dilative point, and (b) softening point.

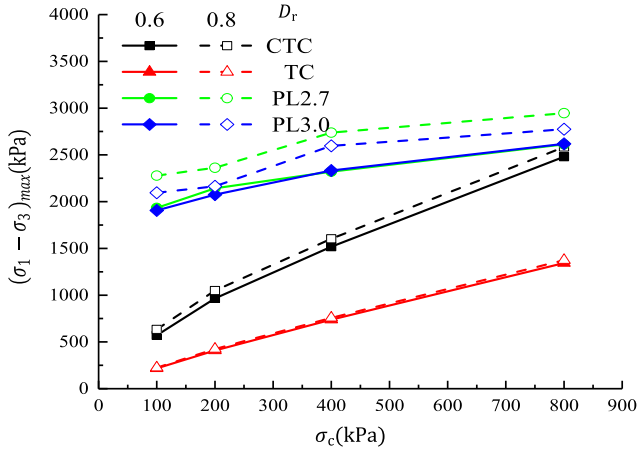

Fig. 9. Deviator stress versus consolidation pressure at the peak point.

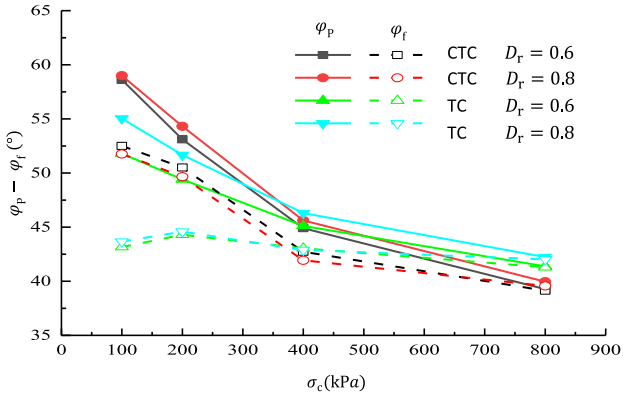

Fig. 10. Peak friction angle φ_p and final friction angle φ_f versus confining pressure.

$$\varphi_p = \varphi_0 - \Delta\varphi \lg\left(\frac{\sigma_c}{P_a}\right), \tag{8}$$

where φ_0 is the friction angle derived from Mohr circle, $\Delta\varphi$ is the change of friction angle due to the increased consolidation stress, and P_a is the atmospheric pressure.

According to the test results, we can get the peak friction angles in the CTC and TC tests:

$$\sigma_p = 60.77^\circ - 23.60^\circ \lg\left(\frac{\sigma_c}{P_a}\right) \text{ (CTC)}, \tag{9}$$

$$\sigma_p = 56.03^\circ - 15.50^\circ \lg\left(\frac{\sigma_c}{P_a}\right) \text{ (TC)}. \tag{10}$$

Figure 11 shows the relationship between the peak friction angle and consolidation pressure of the calcareous sand with the initial relative density of 0.8 in the CTC and TC tests. It is shown that the peak friction angle of the calcareous sand has a linear relationship with the consolidation pressure in both tests. The values of φ_P of the sample with $D_r = 0.8$ are 60.77° in the CTC test and 56.03° in the TC test, but the gradients of the fitting line are different.

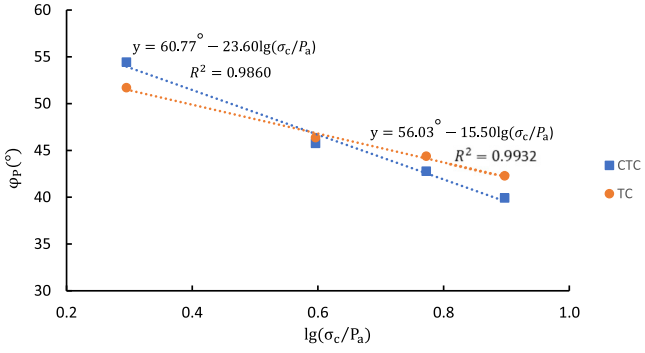

Fig. 11. Relationship between peak friction angle and the consolidation pressure.

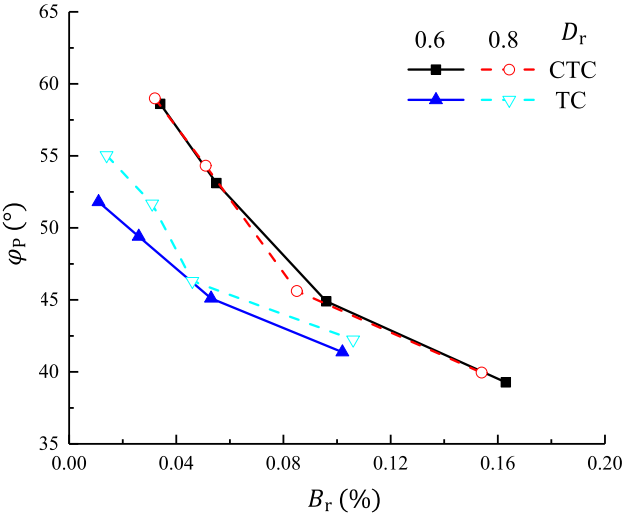

Fig. 12. Friction angle versus the relative breakage potential.

3.3 Breakage potential

To illustrate the relationship between the particle breakage and shear strength of calcareous sand, the friction angle versus the relative breakage potential B_r is plotted in Fig. 12. The value of φ_P decreases with the increase of particle breakage potential. This is different from the behaviour of quartz sand (Guo & Han, 2016). Hence, the effects of consolidation pressures and stress path on the peak friction angle are closely related to the particle breakage. The difference in the degree of particle breakage, denoted as the relative breakage potential B_r, induces the difference in the peak shear strength of calcareous sand.

Figure 13 presents the particle size distribution curves of calcareous sand before and after each test. The calcareous sand with an initial particle size between 1 and 2 mm contains a wide range of particle sizes between 0.075 and 2 mm after shearing due to the particle breakage. However, the majority of particle sizes are larger than 0.25 mm. The den-

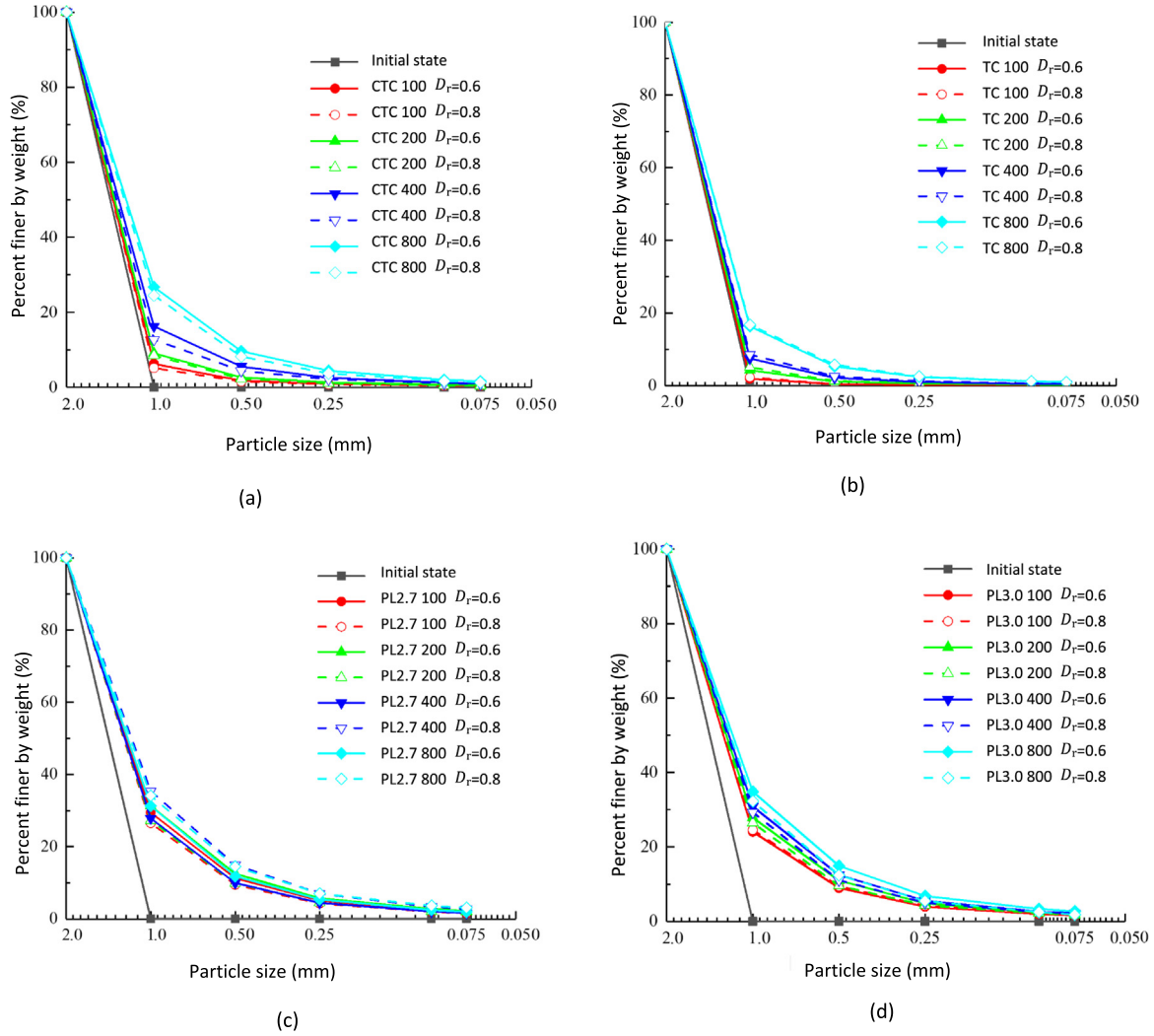

Fig. 13. Particle size distribution curves of calcareous sand before and after each test: (a) CTC, (b) TC, (c) PL2.7, and (d) PL3.0.

ser sand under the higher confining pressure has a smoother concave curve after shearing. In addition, it is shown that the calcareous sand in the PL test contains a wider range of particle sizes compared with that in the other tests. The sand in the TC test tends to have a narrower particle size distribution.

Figure 14 shows the relationship between relative breakage potential and consolidation pressure. In the PL tests the relative breakage potential is the largest compared with that in the CTC and TC tests, and it increases with the principal stress ratio. In the TC and CTC tests, the stresses applied to the calcareous sand are small, leading to relatively weak interlocking between particles. Hence there is a less degree of particle breakage in the TC and CTC tests, and the value of the relative breakage potential is very small. Under the same consolidation pressure, the relative breakage potential increases with the decrease of initial relative density of the calcareous sand. This is because the denser sand is well compacted, and contains more particles in a unit volume. Each particle of denser sand is considered to have more contacted neighbouring particles, thereby limiting and constraining the relative movement of each particle. Less movement leads to less particle breakage.

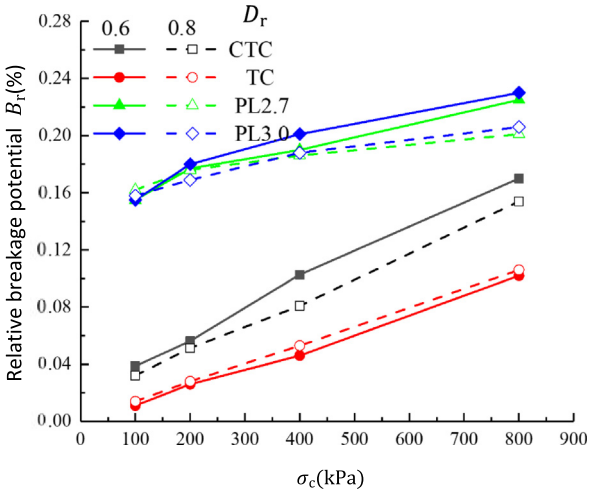

Fig. 14. Relationship between relative breakage potential and the consolidation pressure.

The effect of the stress path on the mechanical properties of calcareous sand can be illustrated by the micro-structure change of calcareous sand, as shown in Fig. 15. As discussed above, the calcareous sand particle in the PL tests broke to a larger extent compared with that in the CTC and TC tests. In the PL2.7 and PL3.0 tests, the porous structures were crushed and the void space was filled with fine particles. These fine particles effectively filled up the void space, so the particles began to rearrange, and new contacts and interlocking developed between the particles. This can be confirmed by the change of particle size distribution, as shown in Fig. 15.

At the same time, the calcareous sand particles formed new micro-structures in the PL2.7 and PL3.0 tests. During this process in the triaxial tests, the original shear strength of the irregular coarse sand particles was gradually replaced by the shear strength of regular fine sand particles (Fig. 16(b)). But in the CTC and TC tests, there were not enough fine particles to form the new strong micro-structure (Fig. 16(a)). Once the initial structure of particles started to break, the residual shear strength decreased continually with the shear strain. Hence, the shear strength of the calcareous sand under different stress paths behaved totally different due to the different micro-structure changes.

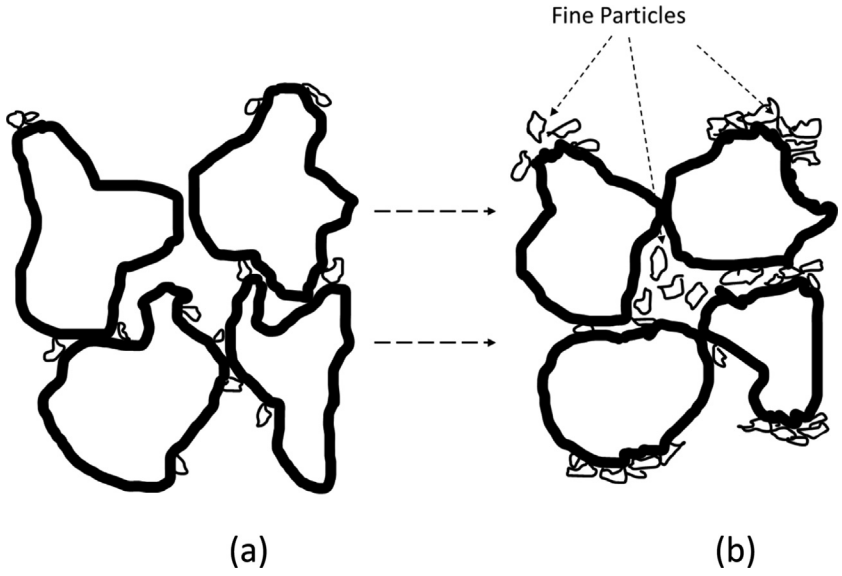

Fig. 15. Concept of particle breakage after triaxial tests under different stress paths: (a) CTC and TC tests, and (b) PL2.7 and PL3.0 tests.

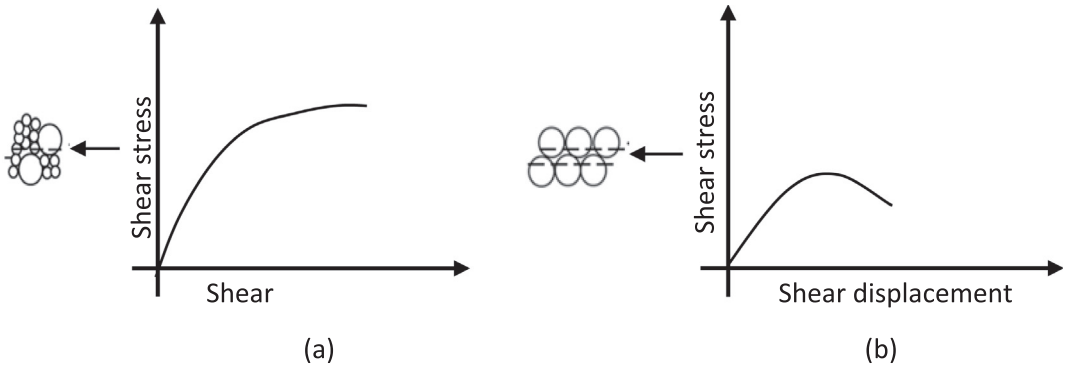

Fig. 16. Effect of particle breakage on the shear strength: (a) CTC and TC tests, and (b) PL2.7 and PL3.0 tests.

4 Conclusion

In this paper, triaxial tests were used to investigate the stress–strain relationship, shear strength, and particle breakage of calcareous sand under the three stress paths CTC, TC and PL. The following main conclusions have been obtained:

(1) The stress path influences the stress–strain relationship and the soil volume change of calcareous sand. The stress–strain showed softening behaviour in the CTC and TC tests, but hardening behaviour in the PL tests. Dilation and compression of the sample were observed in the CTC and TC tests, but only compression occurred in the PL tests. The values of the deviator stress, the axial strain, and the volumetric strain at the softening point (peak point) are higher than the values at the dilation point.

(2) The stress path also influences the shear strength and particle breakage of calcareous sand. Under the same stress path, the sand consolidated by the greater confining pressure tends to have a higher strength and degree of particle breakage. For the same confining pressure, the sand in the PL tests produces a higher strength and degree of particle breakage. Conversely, the lowest strength and degree of particle breakage of the sand were observed in the TC tests. The friction angle of calcareous sand decreased as the particle breakage potential increased. The relationship between the peak friction angle and the confining pressure of the calcareous sand under different stress paths can be presented by an exponential function.

(3) The results show that the confining pressure affects the volumetric change only in the CTC and TC tests. In addition, the dilation behaviour of calcareous sand is more significant under a lower confining pressure. However, for the sand under a higher confining pressure, compression behaviour was seen in the CTC tests. Under the same stress path, the increased confining pressure can lead to greater deviator stresses, peak friction angles and relative breakage potential, as well as smaller final friction angles.

(4) The underlying mechanisms responsible for the different behaviours of calcareous sand observed in this study were discussed. For the calcareous sand in the CTC and TC tests, strain-softening behaviour was observed as the strain continually developed. But for the sand in PL2.7 and PL3.0 tests, the particles tended to rearrange and form new interparticle contacts and interlocking, generating an increase in the residual shear strength. Hence, the shear strength of the calcareous sand under different stress paths behaved totally different due to the different microstructure changes.

Declaration of Competing Interest

The authors declare that they have no known competing financial interests or personal relationships that could have appeared to influence the work reported in this paper.

Acknowledgements

This research was supported by the National Natural Science Foundation of China (Grant Nos. 41877260 and 41772336). All the supports are acknowledged.

References

Altuhafi, F. N., & Coop, M. R. (2011). Changes to particle characteristics associated with the compression of sands. *Géotechnique, 61*(6), 459–471.

Airey, D. W., Carter, J. P., & Liu, M. D. (2011). Sydney soil model. II: Experimental validation. *International Journal of Geomechanics, 11*(3), 225–238.

Bai, Y., & Bai, Q. (2018). *Subsea engineering handbook*. New York: Gulf Professional Publishing.

Chai, W., Long, Z. L., Kuang, D. M., Chen, J. M., & Yan, C. P. (2019). Effect of shear rate on shear strength and deformation characteristics of calcareous sand in direct shear test. *Rock and Soil Mechanics, 40*(s1), 359–366.

Coop, M. R. (1990). The mechanics of uncemented carbonate sands. *Géotechnique, 40*(4), 607–626.

Coop, M. R., & Atkinson, J. H. (1993). The mechanics of cemented carbonate sands. *Géotechnique, 43*(1), 53–67.

Duncan, J. M., & Chang, C. Y. (1970). Nonlinear analysis of stress and strain in soils. *Journal of Soil Mechanics and Foundations Division, 96*(5), 1629–1653.

David Frost, J., Kim, D., & Lee, S. W. (2012). Microscale geomembrane-granular material interactions. *KSCE Journal of Civil Engineering, 16* (1), 79–92.

Einav, I. (2007). Breakage mechanics—Part I: Theory. *Journal of the Mechanics and Physics of Solids, 55*(6), 1274–1297.

Fukuoka, H., Sassa, K., & Wang, G. (2007). Shear behavior and shear zone structure of granular materials in naturally drained ring shear tests. In *Progress in Landslide Science* (pp. 99–111). Berlin, Heidelberg: Springer.

Fahey, M., & Jewell, R. J. (1988). Model pile tests in calcarenite. In R. J. Jewell, & M. S. Khorshid (Eds.). *Proceeding of the International Conference on Calcareous Sediments, Perth. Australia* (2, pp. 555–564). Rotterdam: Balkema.

Guo, Y., & Han, J. (2016). Influence of sampling methods and stress paths on the consolidated undrained shear behaviour of saturated fine sand with medium density. *Chinese Journal of Geotechnical Engineering, 38* (S2), 79–84 (in Chinese).

Hardin, B. O. (1985). Crushing of soil particles. *Journal of Geotechnical Engineering, 111*(10), 1177–1192 (in Chinese).

He, J. Q., Wei, H. Z., Meng, Q. S., Wang, X. Z., & Wei, C. F. (2018). Evolution of particle breakage of calcareous sand under large displacement shearing. *Rock and Soil Mechanics, 39*(1), 165–172.

Jafarian, Y., Javdanian, H., & Haddad, A. (2018). Dynamic properties of calcareous and siliceous sands under isotropic and anisotropic stress conditions. *Soils and Foundations, 58*(1), 172–184.

Miao, G., & Airey, D. (2013). Breakage and ultimate states for a carbonate sand. *Géotechnique, 63*(14), 1221–1229.

Powrie, W. (2004). *Soil Mechanics: Concepts and Applications*. London: CRC Press.

Shahnazari, H., & Rezvani, R. (2013). Effective parameters for the particle breakage of calcareous sands: An experimental study. *Engineering Geology, 159*, 98–105.

Wei, H., Zhao, T., He, J., Meng, Q., & Wang, X. (2018). *Evolution of particle breakage for calcareous sands during ring shear tests*. American Society of Civil Engineers.

Wei, H., Yin, M., Zhao, T., Yan, K., Shen, J., Meng, Q., Wang, X., & He, J. (2021). Effect of particle breakage on the shear strength of calcareous sands. *Marine Geophysical Research, 42*(3), 1–11.

Wu, Y., Yoshimoto, N., Hyodo, M., & Nakata, Y. (2014). Evaluation of crushing stress at critical state of granulated coal ash in triaxial test. *Géotechnique Letters, 4*(4), 337–342.

Yan, C. P., Long, Z. L., Zhou, Y. C., Kuang, D. M., & Chen, J. M. (2020). Investigation on the effects of confining pressure and particle size of shear characteristics of calcareous sand. *Rock and Soil Mechanics, 41*(2), 581–591 (in Chinese).

Yang, C., Wang, K., & Qiao, L. P. (2019). Acoustic emission test of calcareous sands under undrained condition. *Coal Geology & Exploration, 47*(1), 144–148 (in Chinese).

Yu, F. (2017). Particle breakage and the drained shear behavior of sands. *International Journal of Geomechanics, 17*(8), 04017041.

Zhang, J. M., Jiang, G. S., & Wang, R. (2009). Research on influences of particle breakage and dilatancy on shear strength of calcareous sands. *Rock and Soil Mechanics, 30*(7), 2043–2048 (in Chinese).

Zhang, J. M., Zhang, L., Liu, H., Wang, J. J., & Rui, Q. Y. (2008). Experimental research on shear behavior of calcareous sand. *Chinese Journal of Rock Mechanics and Engineering, 27*(S1), 3010–3015 (in Chinese).